Supplementary Information (SI) for New Journal of Chemistry.

Supporting Information

ZIF-L-derived Fe-N-$_{hc}$C Catalysts with Curved Carbon Surfaces for Effective for Oxygen Reduction over the Entire pH Range

Xu Dai [a] and Zhenlu Zhao [a, b] *

[a] *School of Material Science and Engineering, University of Jinan, Jinan 250022, Shandong, China.*

[b] *State Key Lab of Electroanalytical Chemistry, Changchun Institute of Applied Chemistry, Chinese Academy of Sciences, Changchun 130022, Jilin, China*

E-mail: mse_zhaozl@ujn.edu.cn

Materials and chemicals

Ferric citrate, Zinc nitrate hexahydrate [Zn $(NO_3)_2 \cdot 6H_2O$] and 2-Methylimidazole (98%) were purchased from Sigma-Aldrich. Triblock copolymers poly (ethylene oxide)-b-poly (propylene oxide)-b-poly (ethylene oxide) Pluronic®P123 ($PEO_{20}PPO_{70}PEO_{20}$, Mw = 5800) and Pt/C (20wt%) were purchased from Shang Hai Maclean Biochemical Co. Nafion® solution (5 wt%) was purchased from Energy Chemical. The deionized water was made by the laboratory water purifier (18.3 MΩ cm). All the chemicals used in the synthesis of catalysts were analytical purity and no further purification was made.

1. Characterizations

The morphology and size of the catalysts were characterized by field emission scanning electron microscopy (SEM, Gemini300) and high-resolution transmission electron microscopy (HR-TEM, JEOL JEM-F200). Further surface characterization of the catalysts was measured by atomic force microscopy AFM (Bruker Dimension ICON). The crystal structure information was obtained by X-ray diffraction (XRD, Japan Rigaku Smart Lab SE) with Cu Ka radiation (λ = 0.15 nm) in the 2θ range from 5° to 80°. The composition, chemical state, and molecular structure of elements on the surface of the sample were obtained by X-ray photoelectron spectroscopy (XPS, Thermo Scientific ESCALAB Xi^+). The degree of disorder and graphitization of the sample carbon were measured using a 532 nm laser as the excitation source using a Raman spectrometer (HR Evolution). Nitrogen adsorption-desorption measurements on MAC TriStar II 3flex. The pore size distribution and specific surface area of the sample were determined by Brunauer-Emmett-Teller (BET) method. The specific element content was determined by an inductively coupled plasma spectrum/mass spectrometer (Agilent 5110(OES).

2. Electrochemical measurements

All ORR electrochemical measurements were performed on the CHI 760E electrochemical workstation via a three-electrode cell with a Hg/HgO as a reference electrode, a graphite rod as a counter electrode, and an electrocatalyst-coated rotating disk electrode as a working electrode. A uniform electrocatalyst ink was prepared by ultrasonically dispersing 5.0 mg electrocatalyst powder in a mixed solution containing 1ml ethanol and 2μL Nafion for 1h. Cyclic voltammetry curves (CV) and linear sweep voltammetry curves (LSV) are obtained at a sweep rate of 10 mV s^{-1} and 2 mV s^{-1} over a potential range of 0 to 1.2 V. Long-term stability and CH_3OH (1 M) toxicity tests were performed by measuring current-time (I-t) chrono current response at 0.7 V and 1600 rpm. To further calculate the electron transfer number (n), the Koutecky-Levich (K-L) equation is as follows:

$$J^{-1} = J_k^{-1} + B^{-1}\omega^{-\frac{1}{2}}$$

$$B = 0.2nFC_0D_0^{\frac{2}{3}}V^{-\frac{1}{6}}$$

where J and J_k are the measured and kinetic current densities, respectively, ω is the rotating speed, n is the electron transfer number, F is the Faraday constant (96,485 C mol^{-1}), C_0 is the bulk concentration of oxygen (1.2×10^{-6} mol cm^{-3}), D_0 is the diffusion coefficient of oxygen (1.9×10^{-5} cm^2 s^{-1}), and V is the kinematic viscosity of the electrolyte (0.01 cm^2 s^{-1}).

The electron transfer number (n) and yield of peroxide can be evaluated from the LSV curve of RRDE measurement at 1600 rpm according to the following equation:

$$n = \frac{4 \times I_D}{I_D + I_R/N}$$

$$H_2O_2(\%) = 200\frac{I_R/N}{I_D + (I_R/N)}$$

where I_D represents disk current and I_R represents ring current at 1.23 V vs RHE. N = 0.37 is the current collection efficiency of the ring electrode.

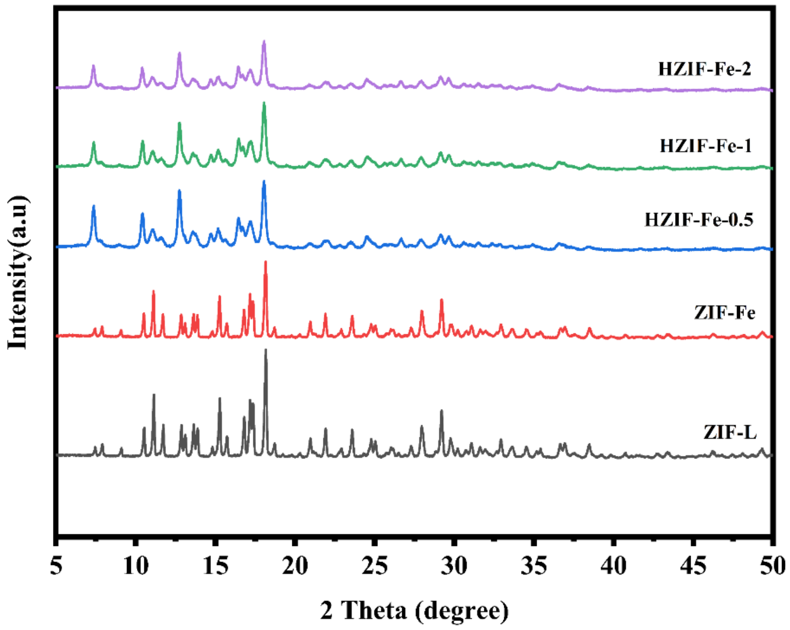

Figure. S1. XRD patterns of ZIF-L, ZIF-Fe, HZIF-Fe-0.5, HZIF-Fe-1, HZIF-Fe-2.

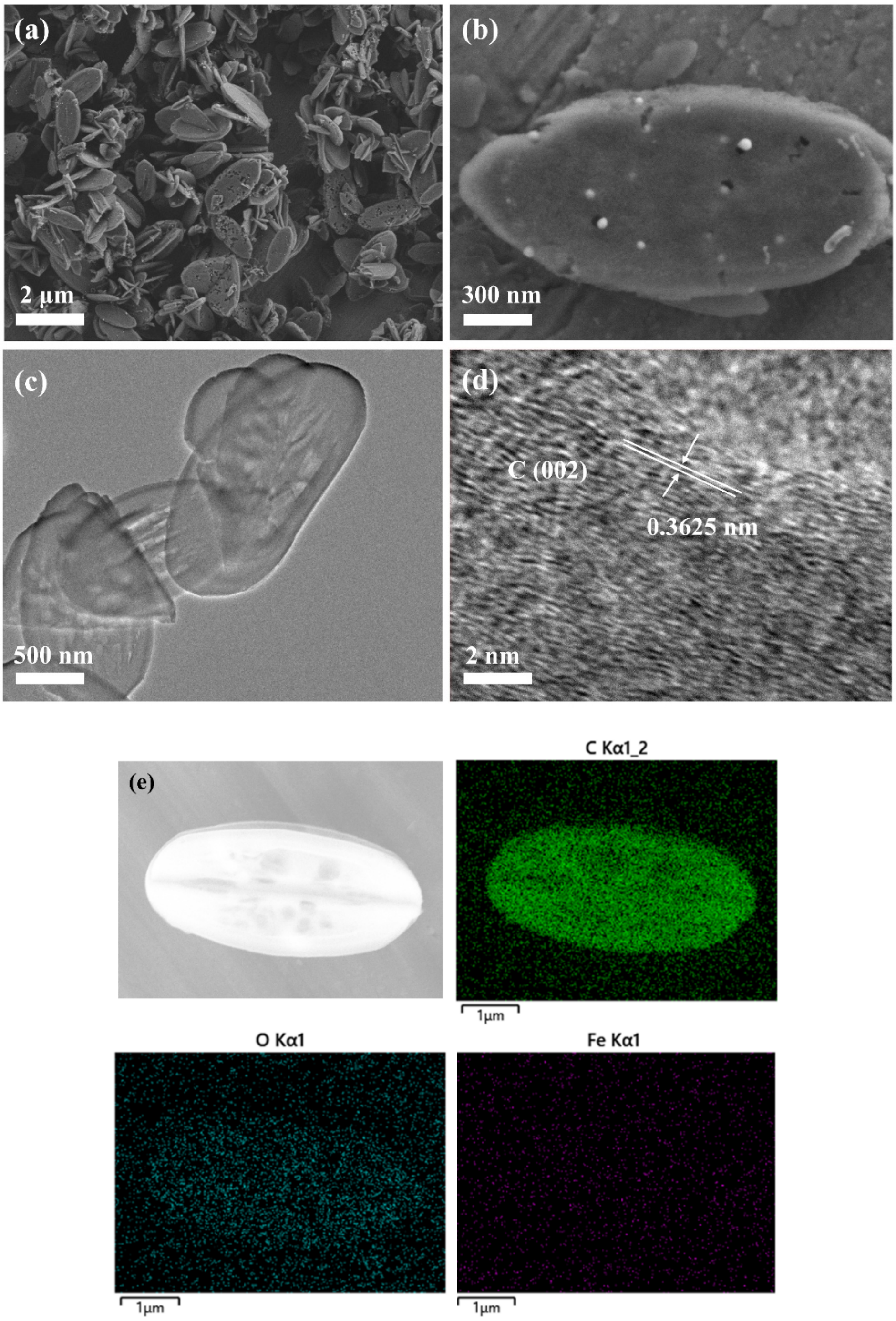

Figure. S2. (a) and (b) SEM images of FeN-C. (c) TEM images of FeN-C. (d) HR-TEM images of FeN-C. (e) EDS images of FeN-C

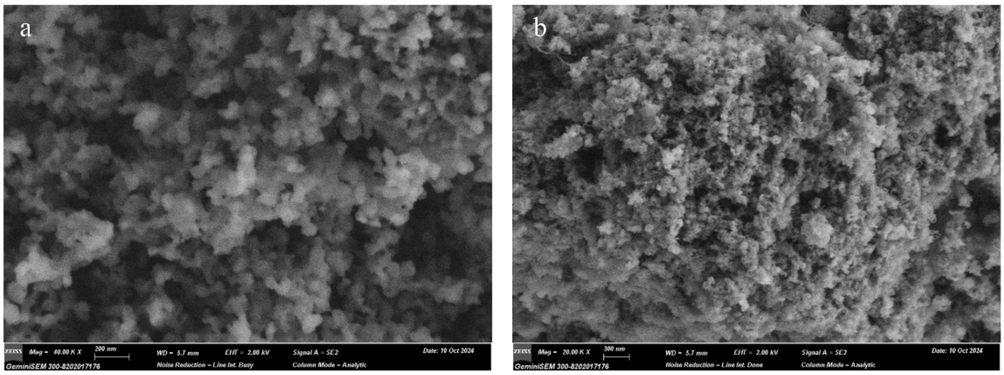

Figure. S3. (a) SEM images of FeN-$_{hc}$C-0.5. (b) SEM images of FeN-$_{hc}$C-2.

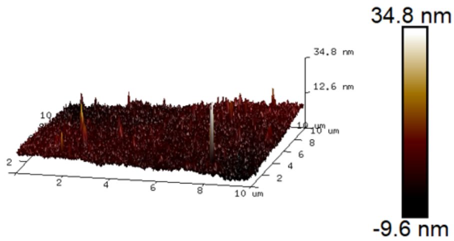

Figure. S4. Atomic Force Microscopy (AFM) image of FeN-$_{hc}$C-1 Catalyst surface.

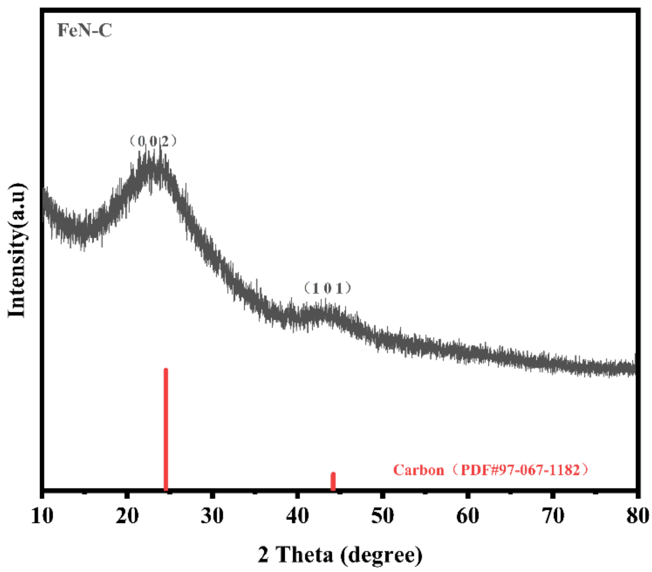

Figure. S5. XRD patterns of FeN-C.

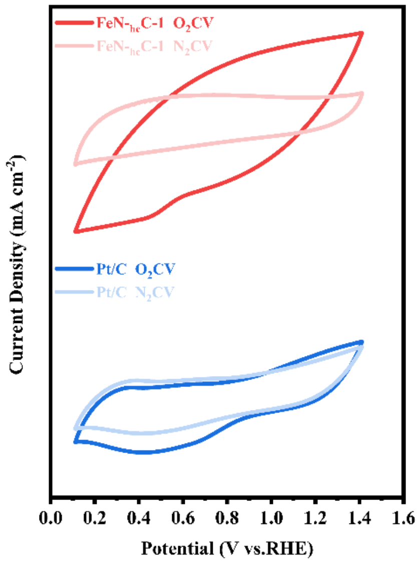

Figure. S6. CV curve of FeN-$_{hc}$C-1and Pt/C under neutral condition.

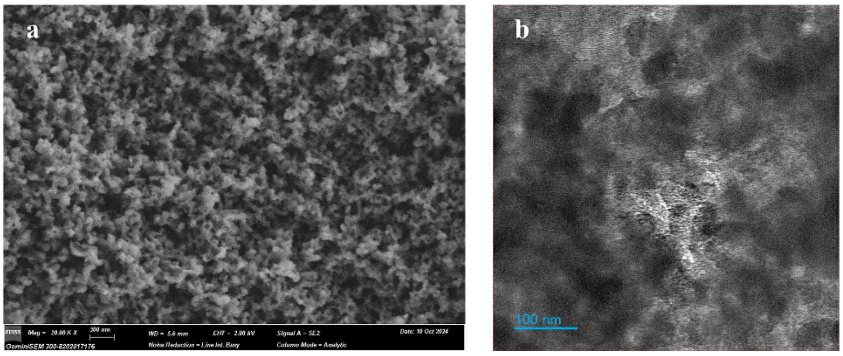

Figure. S7. (a) SEM image of FeN-$_{hc}$C-1 catalyst after stability test. (b) TEM image of FeN-$_{hc}$C-1 catalyst after stability test.

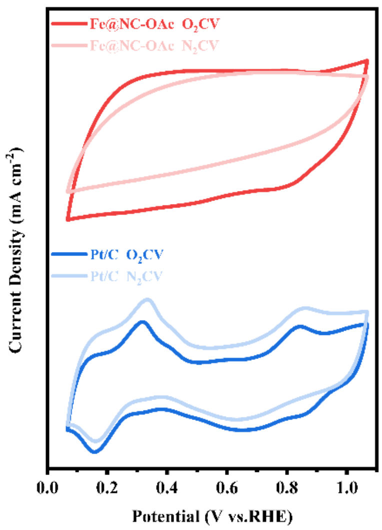

Figure. S8. CV curve of FeN-$_{hc}$C-1and Pt/C under alkaline condition.

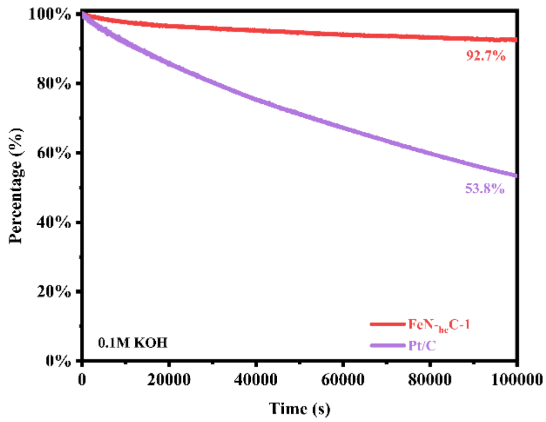

Figure. S9. Stability test curves of FeN-$_{hc}$C-1 and Pt/C at potential of 0.7V in an alkaline electrolyte.

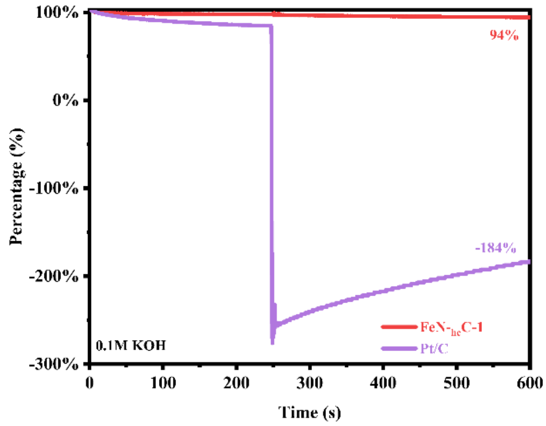

Figure. S10. Curves of methanol tolerance test FeN-$_{hc}$C-1 and Pt/C in alkaline electrolytes.

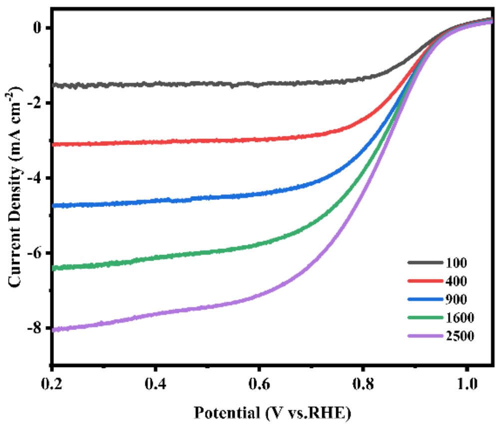

Figure. S11. LSV curves of FeN-$_{hc}$C-1 in alkaline electrolyte at different rotational speeds.

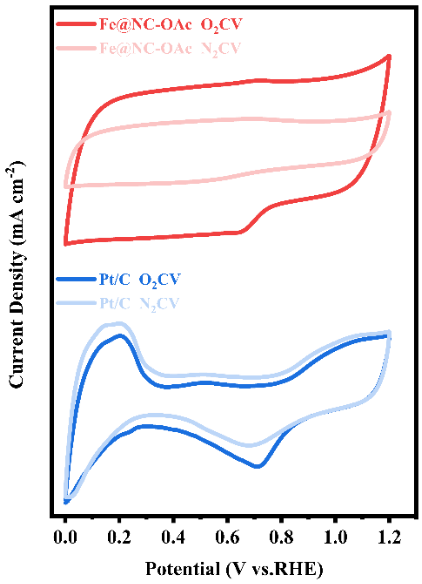

Figure. S12. CV curve of FeN-$_{hc}$C-1and Pt/C under acidic condition.

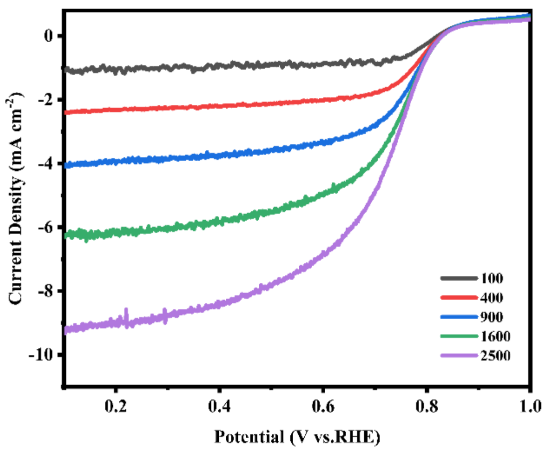

Figure. S13. LSV curves FeN-$_{hc}$C-1 in acid electrolyte at different rotational speeds.

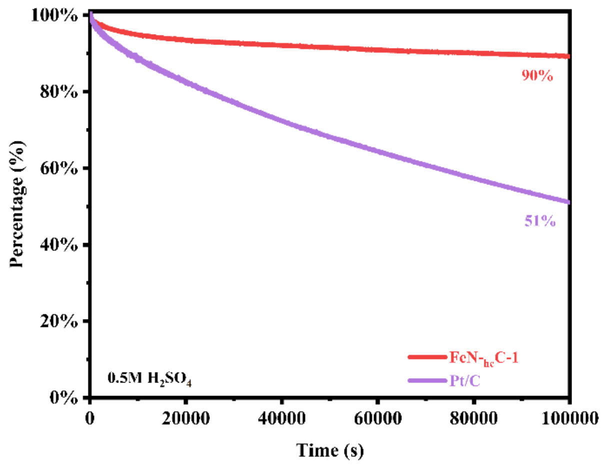

Figure. S14. Stability test curves of FeN-$_{hc}$C-1 and Pt/C at potential of 0.7V in an acid electrolyte.

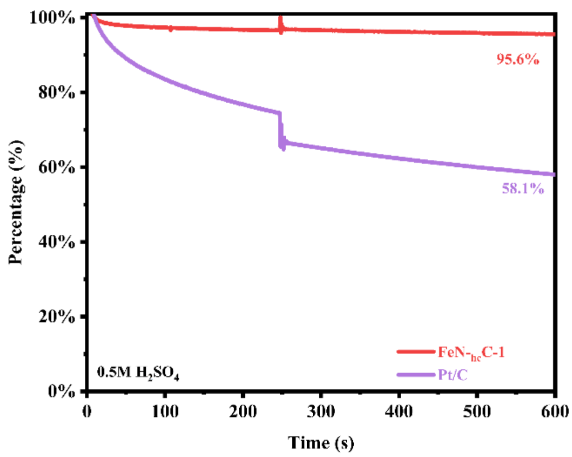

Figure. S15. Curves of methanol tolerance test FeN-$_{hc}$C-1 and Pt/C in acid electrolytes.

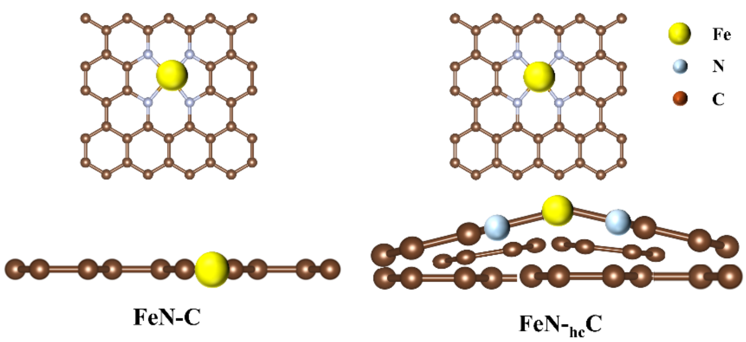

Figure S16. models of FeN-C and FeN-$_{hc}$C.

Table S1. The results of ICP-MS test showed the Fe content in FeN-$_{hc}$C-1 and FeN-C.

Sample name	Test element	Sample element content W (%)
FeN-$_{hc}$C-1	**Fe**	**1.815%**
FeN-C	**Fe**	**1.078%**

Table S2. The XPS test results showed the Fe content on the surface of FeN-$_{hc}$C-1 and FeN-C catalysts.

Sample name	Test element	Sample element content W (%)
FeN-$_{hc}$C-1	**Fe**	**0.53%**
FeN-C	**Fe**	**0.34%**

Table S3. The XPS test results showed the N content on the surface of FeN-$_{hc}$C-1 and FeN-C catalysts.

Sample name	Test element	Sample element content W (%)
FeN-$_{hc}$C-1	**N**	**7.33%**
FeN-C	**N**	**5.56%**

Table S4. Comparison with recently reported catalysts under alkaline conditions.

catalyst	$\mathbf{E_{1/2}}$	**reference**
FeN-$_{hc}$C-1 (This work)	0.89V	/
Fe-N_4S_1	0.88V	[1]
Fe-N-C-300	0.81V	[2]
Fe-NC-Gs	0.85V	[3]
Fe-NPC	0.872V	[4]
FeCoNi/NC	0.84V	[5]

Table S5. Comparison with recently reported catalysts under acidic conditions.

catalyst	$\mathbf{E_{1/2}}$	**reference**
FeN-$_{hc}$C-1 (This work)	0.77V	/
$Nb_{10}Fe_x$/Z8C	0.75V	[6]
FeCr-N-C	0.73V	[7]
Co@N–C-700	0.65V	[8]
CoSA-C_2N	0.74V	[9]
L_FeMn	0.76V	[10]

reference

1. Y. Zhang, C. Li, J. Li, X. Liu, G. Li, B. Li and L. Wang, *J. Mater. Chem. A*, 2023, **11**, 11326-11333.
2. S. Liu, Q. Meyer, Y. Li, T. Zhao, Z. Su, K. Ching and C. Zhao, *Chem. Commun.*, 2022, **58**, 2323-2326.
3. Y. Zhang, P. He, D. Zhuo, J. Zhang, N. Zhang, X. Wang, G. Lin and Z. Kong, *Electron. Mater. Lett.*, 2024, **20**, 95-101.
4. L. Zhang, Z. Shen, X. Lu, X. Jiao and G. He, *Mater. Lett.*, 2023, **341**, 134237.
5. H. Huang, C. Zhang, H. Li, J. Wang, Z. Chen, Y. He, Y. Li, J. Hu, X. Liu, X. Deng and S. Shi, *Catalysis Science & Technology*, 2024, **14**, 2638-2645.
6. J. Luo, Z. Lu, Y. Zhang, D. Wu, D. Dang, N. Yu, Y. Xu, S. Feng, S. Wang, Z. Zhang, Y. Zhao, P. Deng, J. Li, Z. Miao and X. Tian, *Materials Today Nano*, 2024, **25**, 100448.
7. N. Xue, Y. Zhang, C. Wang, X. Xue, D. Ouyang, H. Zhu and J. Yin, *Int. J. Hydrogen Energy*, 2022, **47**, 33979-33987.
8. S. Chen, Q. Xu, H. Sun, L. Ge, D. Huang, Z. Zhang, Y. Qiao, X. Tong and W. Fan, *ACS Appl. Nano Mater.*, 2024, **7**, 15710-15719.
9. W. Xu, Y. Sun, J. Zhou, M. Cao, J. Luo, H. Mao, P. Hu, H. Gu, H. Zhai, H. Shang and Z. Cai, *Nano Res.*, 2023, **16**, 2294-2301.
10. M. Muhyuddin, A. Friedman, F. Poli, E. Petri, H. Honig, F. Basile, A. Fasolini, R. Lorenzi, E. Berretti, M. Bellini, A. Lavacchi, L. Elbaz, C. Santoro and F. Soavi, *J. Power Sources*, 2023, **556**, 232416.